PCCP

Accepted Manuscript

This is an *Accepted Manuscript*, which has been through the Royal Society of Chemistry peer review process and has been accepted for publication.

Accepted Manuscripts are published online shortly after acceptance, before technical editing, formatting and proof reading. Using this free service, authors can make their results available to the community, in citable form, before we publish the edited article. We will replace this *Accepted Manuscript* with the edited and formatted *Advance Article* as soon as it is available.

You can find more information about *Accepted Manuscripts* in the **Information for Authors**.

Mesoscopic modeling of structural and thermodynamic properties of fluids confined by rough surfaces

Ketzasmin A. Terrón-Mejía, Roberto López-Rendón

Laboratorio de Bioingeniería Molecular a Multiescala, Facultad de Ciencias,
Universidad Autónoma del Estado de México,
Av. Instituto Literario 100, 50000, Toluca, México

Armando Gama Goicochea[*]
Instituto de Física, Universidad Autónoma de San Luis Potosí,
Av. Álvaro Obregón 64, 78000, San Luis Potosí, México

Abstract

The interfacial and structural properties of fluids confined by surfaces of different geometry are studied at the mesoscopic scale using dissipative particle dynamics simulations in the grand canonical ensemble. The structure of the surfaces is modeled by a simple function, which allows us to simulate readily different types of surfaces through the choice of three parameters only. The fluids we have modeled are confined either by two smooth surfaces or by symmetrically and asymmetrically structured walls. We calculate structural and thermodynamic properties such as the density, temperature and pressure profiles, as well as the interfacial tension profiles for each case and find that a structural order − disorder phase transition occurs as the degree of surface roughness is increased. However, the magnitude of the interfacial tension is insensitive to structuring of the surfaces and depends solely on the magnitude of the solid − fluid interaction. These results are important for modern nanotechnology applications, such as in the enhanced recovery of oil, and in the design of porous materials with specifically tailored properties.

Keywords: symmetrically and asymmetrically structured surfaces; interfacial tension profile; dissipative particle dynamics.

---

[*] Corresponding author. Electronic mail: agama@alumni.stanford.edu

I. INTRODUCTION

The research progress in the science and technology of nanoscale systems in recent years poses new challenges for the understanding of the properties of materials at this scale and the mechanisms that give rise to those properties from a more fundamental point of view. In particular, liquids are known to exhibit completely different behavior when they are confined at the molecular range [1]. The study of thermodynamics and structural properties of confined fluids by surfaces of different morphologies, especially at the nanometer scale, is especially important for many industrial and bioengineering applications. For example, nanorheology has received increasing attention over the past two decades, with important advances in nanomaterials, microfluidics, and nanofluidics, providing significant insights into various applications such as boundary lubrication, adhesion, adsorption, and wetting, in technologies such as catalysis, gas adsorption, boundary lubrication, adhesion and oil recovery, to name a few [2]. One of the most challenging unresolved issues is to elucidate the relationship between the rheological properties and the structural evolution of confined fluid films and particles' suspensions [3]. Two major experimental techniques for studying the rheological behavior of confined liquids include atomic force microscopy (AFM) and the surface forces apparatus (SFA) [4-7]. AFM and SFA have been widely used to measure normal and lateral forces between a tip (a colloidal probe) and a flat surface (with AFM) or between two curved surfaces (with SFA) with high precision. In most of these studies, the fluid is bound by naturally occurring surfaces, which are rough and/or energetically inhomogeneous, and the heterogeneity leads to an enhancement of adsorption under quite general conditions. Despite the significant progress achieved with these techniques, there are still many remaining challenges in the field. For example, it is still experimentally challenging to determine the detailed structural information of

confined fluids in many systems. Surface roughness occurs in a wide variety of processes where it is both difficult to avoid and control. When two bodies are separated by a small distance the roughness starts to play an important role in the interaction between the bodies, their adhesion, and friction. It has been found also that even small differences in the roughness morphology lead to observable changes in the force profiles [8].

It is known that fluids confined within narrow pores can display drastically different phase behavior from that of the bulk fluid [9]. Such confinement – driven phase changes can be attributed to a combination of the effects of the fluid – surface interaction [10]. This phenomenon has been widely examined experimentally, and there is strong evidence of confinement – induced solidification [11]. Currently, there is no agreement as to the nature of the transition, in large part due to the intrinsic difficulties faced in experiment, i.e., it has not yet been possible to observe directly the structure within the pores. Following the initial observation of nanoconfinement – induced solidification by Gee and co-workers using the SFA [12], surface force balance experiments carried out by Klein and co-workers on simple organic solvents nanoconfined between two atomically smooth mica surfaces suggest a first – order phase change when the pore separation is reduced from seven to six molecular layers [13]. However, experiments by Demirel and co – workers using the SFA instead suggest a second – order transition [14]. No agreement has yet been reached between these two results, in large part due to the intrinsic difficulties faced in experiments at those scales [15]. More recent experiments have provided additional insights into this debate; several studies have found results consistent with the work of Klein and Kumacheva [16], while others have shown agreement with the conclusions of Demirel et al. [17]. On the other hand, very few experimental studies have concentrated on investigating the influence of roughness on boundary slip. These experiments are challenging chiefly because of it

is difficult to produce suitable surfaces of controlled roughness. Most efforts to alter the surface roughness result in additional undesired changes to the interface properties. The interpretation of the results is complicated by the uncertainty in the wall position that is associated with roughness. An appropriate theoretical description of realistic surface roughness is yet to be found [18]. In the engineering community, the effect of surface roughness on the flow of simple liquids in microchannels has been thoroughly investigated, but a model valid to explain all experiments has not been proposed (see [19, 20] and references therein).

A variety of molecular simulation schemes have been used to study phase transitions in confined systems. The principal methods used are grand canonical Monte Carlo (GCMC) simulation and Gibbs ensemble Monte Carlo (GEMC) simulation [21-22]. Other methods that have been applied less frequently to these problems are semi-grand Monte Carlo (SGMC), histogram – reweighting and histogram – biasing methods [23-24]. GCMC simulations, which keep the chemical potential, volume and temperature constant during the simulation, are ideally suited to model confined fluids because chemical equilibrium plays the key role in determining phase equilibrium between the fluid in the confined region and the bulk fluid. The choice of the GCMC technique is dictated by the conditions of AFM and SFA experiments, where the confined fluid is open to the bulk fluid reservoir. Among its advantages over other techniques is its ability to incorporate density fluctuations while keeping the chemical potential fixed, which is crucial to keep confined fluids in thermodynamic equilibrium with the bulk. Using GCMC, the phase diagram of a Lennard-Jones fluid confined by a quenched disordered structure was studied by De Grandis and collaborators [25]. Gruhn *et al.* investigated the microscopic structure of liquid-crystalline films confined between two plane parallel solid surfaces (i.e. walls) consisting of discrete, rigidly fixed atoms distributed across the plane of a wall [26]. The effect of branching

on the structure of confined thin films of alkanes was studied by Dijkstra through GCMC simulations [27]. Extensive GCMC simulations have been conducted by Porcheron *et al.* [28 – 30] to study the effect of wall corrugation on the confined fluid structure. They used furrowed slits to model surface roughness effects at the nanometer scale, while the confining walls remained smooth on the atomistic scale. It has been shown that the fluid confined between planar walls exhibits a damped oscillatory solvation pressure profile. A transition from oscillatory to non – oscillatory behavior is observed when the characteristic length of the furrow reaches the length of the anisotropic *n*-butane [31] molecule.

However, simulating the thermodynamics of fluids confined by rough surfaces with atomistic detail is still rather demanding computationally, especially if one is interested in modeling large systems. It is well established that for a fluid confined by pores larger than a few nanometers its thermodynamic properties far from the matrix wall are close to its bulk properties. If one is primarily interested in global rather than in local properties, it may be useful to introduce surface quantities to characterize the difference between the adsorbed and bulk fluids [32]. An alternative approach is the use of mesoscopic, coarse–grained techniques that incorporate particles that are large enough for external (hydrodynamic) forces to influence their dynamics but not so large that thermal (Brownian) forces are negligible. Dissipative particle dynamics (DPD) is one of those mesoscopic techniques and has been shown to be successful in the prediction of equilibrium and non-equilibrium properties of soft matter systems [33-34]. Implementation of wall or solid objects in DPD is an issue that needs to be addressed carefully; a simple way to incorporate a solid object is to freeze locally the portions of the fluid [35-36]. Due to the soft interaction potential, particles may penetrate the wall creating slip. To prevent this, a higher wall density is necessary, increasing the computational demand, but increasing the wall

density tends to distort the flow field near the wall [37]. However, most simulations of confined fluids with DPD have been carried out only for smooth and homogeneous walls [38-40]; to our knowledge, the properties of fluids confined by rough surfaces have not yet been studied at the mesoscopic scale. Among the few reports on this topic is that of Liu *et al*. [41], who studied the morphology in aqueous solutions of a nonionic triblock copolymer, using mesoscopic dynamics. Liu and Jiang have published a review that focuses on the recent progress in mechanisms, preparation, and applications of self-cleaning surfaces, where our work can have potential applications [42]. DPD has been shown to be a very useful alternative for the prediction and interpretation of soft matter phenomena when the atomistic details of the system are not important. There are, of course, phenomena that fall beyond the scope of DPD, such as those that require of the simultaneous presence of attractive and repulsive interactions, which are responsible for capillary condensation for example [43]. In this work, we present DPD simulations of fluids confined by structured surfaces with the purpose of predicting their interfacial properties.

The remainder of this paper is organized as follows. The general equations of the DPD approach, the simulation methodology, and our model for rough surfaces are presented and explained in Section II. The details of the simulations are presented in Section III. In Section IV, we present our results for two case studies: (a) the effect of varying the roughness parameter, and (b) the influence of the wavelength of the oscillations on the structural and thermodynamic properties of the fluid. Finally, the conclusions are drawn in Section V.

II. MODELS AND METHODS

A. Dissipative particle dynamics for confined fluids

In the DPD model, the particles do not represent actual molecules but rather groups of molecules with soft boundaries, which is why this is a coarse–grained approach. The theoretical foundations of the DPD method can be found in various sources [44-48], therefore we shall only outline some general aspects of this technique. The idea behind DPD simulations is similar to a traditional MD algorithm [49] in the sense that one must integrate Newton's second law of motion using finite time steps to obtain the particles' positions and momenta from the total force. A difference from atomistic MD is that the DPD model involves not only a conservative force ($\mathbf{F}^{C}$), but also random ($\mathbf{F}^{R}$), and dissipative ($\mathbf{F}^{D}$), components acting between any two particles i and j, placed a distance r_{ij} apart. In its traditional form, the DPD total force is the sum of these three components [44], but to simulate the confinement of DPD fluids by effective surfaces one should include a fourth force to take into account the fluid-wall interactions; we shall call this force ($\mathbf{F}^{W}$), therefore, the total force for confined fluids is the sum of these four components:

$$\mathbf{F}_{ij} = \sum_{i \neq j}^{N}\left[\mathbf{F}^{C}\left(\mathbf{r}_{ij}\right) + \mathbf{F}^{R}\left(\mathbf{r}_{ij}\right) + \mathbf{F}^{D}\left(\mathbf{r}_{ij}\right)\right] + \sum_{i}^{N}\mathbf{F}^{W}(z_{iw}) \quad , \tag{1}$$

All forces between particles i and j are zero beyond a finite cutoff radius r_c, which represents the intrinsic length scale of the DPD model and is usually also chosen as $r_c \equiv 1$. The conservative force determines the thermodynamics of the DPD system and is defined by a soft, linearly decaying repulsion whose maximum strength is given by a constant, a_{ij}. The strength of the dissipative (γ) and random forces (σ) are related in a way that keeps the temperature internally fixed, $k_B T = \frac{\sigma^2}{2\gamma}$; k_B being Boltzmann's constant [44]. At interparticle distances larger than r_c, all forces are equal to zero. This simple distance dependence of the forces, which is a good

approximation to the one obtained by spatially averaging a van der Waals – type interaction [50], allows one to use relatively large integration time steps. The natural probability distribution function of the DPD model is that of the canonical ensemble, where N (the total particle number), V, and T are kept constant.

A salient feature of the last term in eq. 1 is that it depends only on the z coordinate. This force allows us to model the confining surfaces with different geometries, which we design as either smooth, flat walls, or symmetrically and asymmetrically structured surfaces. The modeling of roughness in our simulations can be introduced through this force. To this end, we choose a periodic, symmetric function having the form [51]:

$$\mathbf{F}^{W}(z_{iw}) = a_{w-ie}\left(1 - \frac{z_{iw}}{z_c}\right)\hat{\mathbf{e}}_z \qquad z < z_c, \tag{2}$$

which is zero for $z > z_c$, where z_c is the cutoff distance along the z–axis beyond which the force in eq. 2 is zero; and $\hat{\mathbf{e}}_z$ is a unit vector that points in the z – direction. We have chosen a model for the force that structured walls exert on the fluid that depends only on the z – coordinate because there are periodic boundary conditions along the x – and y – directions. The structure of the walls on the xy – plane is likely to induce some structure locally in the fluid particles more closely adsorbed on the walls, on the xy – plane , but that structure is expected to be a secondary effect compared with the influence of the structure along the z – direction, due to the fact that the fluid is effectively infinite along the x – and y – directions. Equation 2 has two parameters: a_{w-ie} and z_{iw}. The first, a_{w-ie}, is the one that defines the intensity of the repulsive interaction between the walls (w) and the confined fluid species (ie), which may be solvent particles or polymer's monomers for example. Large values of a_{w-ie}, lead to hard walls, while small values of a_{w-ie}

lead to soft walls. The second term, z_{iw}, has two meanings; first, it is a function that takes into account the distance of separation between a fluid's particle (i) and a *planar* wall (w) upon which a structured wall is constructed; secondly, it represents the distance along the z–axis between a given fluid particle and the *structured* surface (the last term in eq. 3) . It is given by

$$z_{iw} = z_i \pm z_w \pm a_R \exp^{[\lambda_2(x_i+y_i)]} \cos\left(\frac{2\pi x_i}{\lambda_1}\right) \cos\left(\frac{2\pi y_i}{\lambda_1}\right) , \tag{3}$$

where z_i and z_w are the position of the particle i and the z–coordinate of the wall w, respectively, whereas x_i and y_i are the position of the particle i in the x and y axes, respectively. The constant a_R is the parameter that controls the amplitude of the roughness on the wall; when $a_R = 0$ one recovers a smooth wall, while for $a_R = 1$ we obtain a rough wall. Furthermore, λ_1 is the parameter that determines the periodicity of the structure on the walls, and λ_2 represents the asymmetry of the structure. Table I summarizes the information that characterizes the different types of surfaces obtained from eq. 3. Figure 1 shows a schematic representation of eq. 3, as a function of the parameters a_R and λ_1, for the particular case when $\lambda_2 = 0$.

Table I. Characteristics of the surfaces modeled in this work

a_R	λ_1	λ_2	Geometry of the surface.
0	Π	0	Smooth wall.
1	Π	0	Symmetrically structured wall.
1	Π	>0	Asymmetrically structured wall
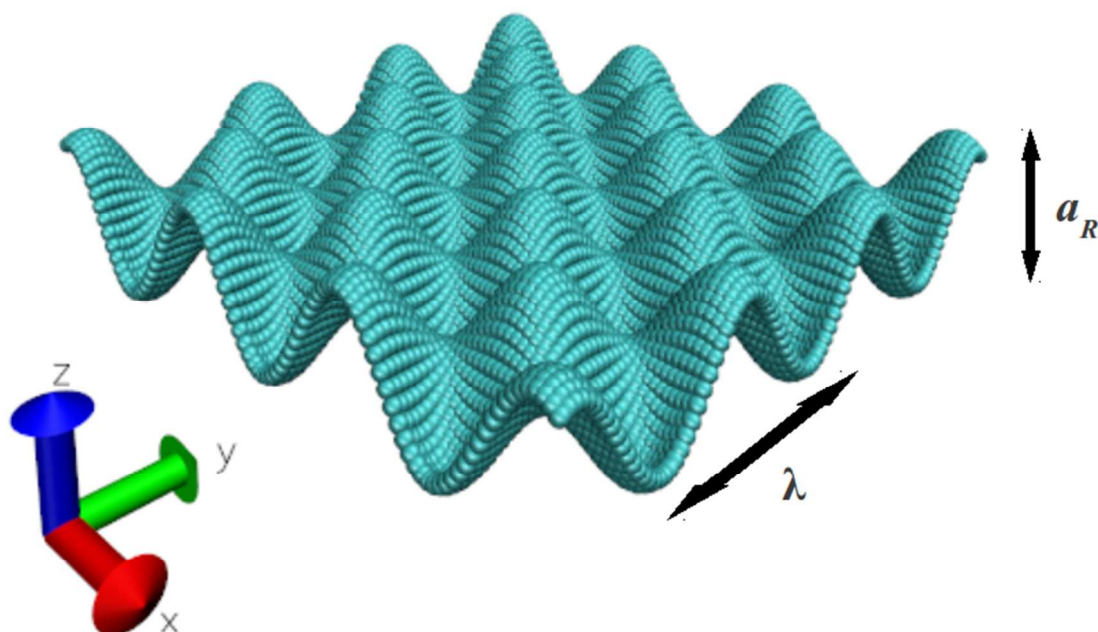
Figure 1. Schematic representation of surface roughness modeled in this work. λ and a_R are parameters that control the oscillation period of the roughness and the amplitude of the structure, respectively. For this figure we used $\lambda \equiv \lambda_1 = \pi$ and $a_R = 1$; $\lambda_2 = 0$. See the discussion of eq. 3. This image was obtained using VMD [52].

In Fig. 1 we show a typical example of the kind of structured wall we have modeled in the work reported here, which is completely characterized by a_R and λ_1. Changing these parameters allows us to set up periodically structured walls or asymmetric walls as well as combinations between those cases, as we have two walls confining the fluid.
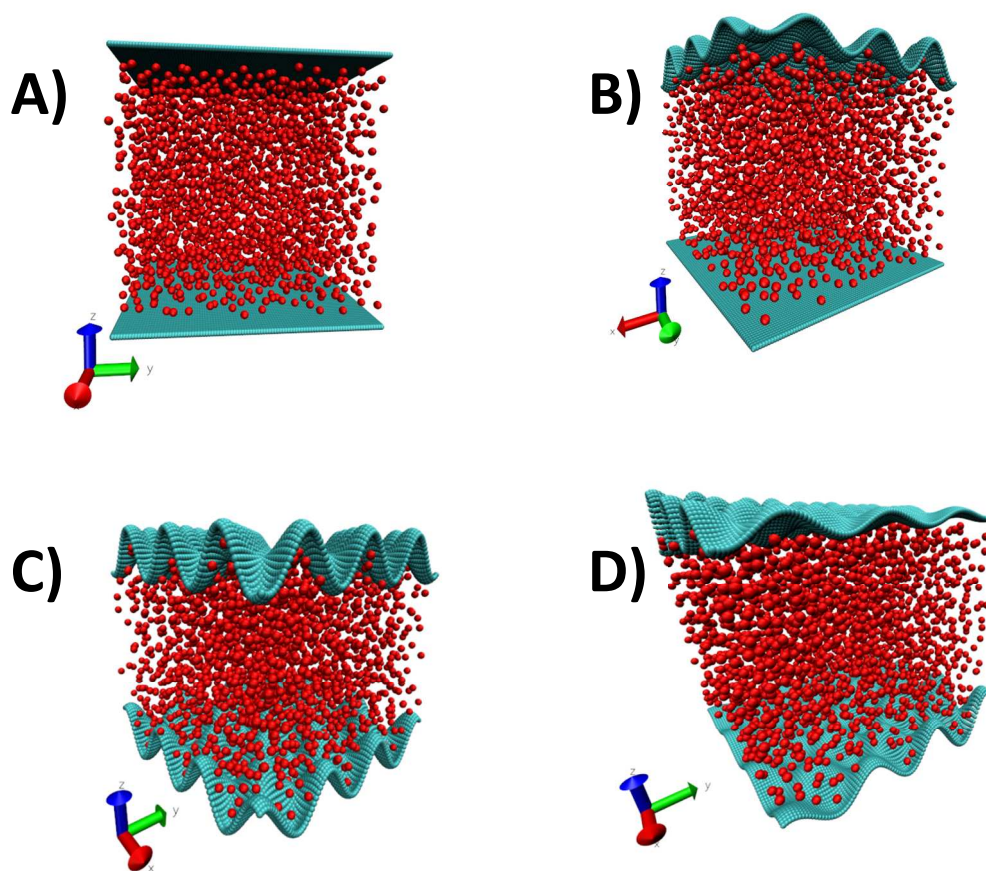
Figure 2. Three-dimensional (3D) views of the different geometries of surfaces studied in this work. The fluid is represented by red particles. Snapshots of the fluid confined by: A) two smooth, planar surfaces (SS); B) a smooth and a symmetrically rough surface (SR); C) two symmetrically rough surfaces (RR); and D) a combination of a two asymmetrically rough surfaces (AA). These images were obtained with VMD [52].

Figure 2 displays all the differently confined systems we research and report here, which include the symmetrical flat surfaces case (Fig. 2(A)); an asymmetrical case where one surface is smooth and the other is a symmetrically structured wall (Fig. 2(B)); when both surfaces are equally structured, the fluid is represented in Fig. 2(C). Finally, we modeled also the case when the fluid is flanked by walls that are not periodically structured but are instead asymmetrically rough (on the xy – plane), as shown in Fig. 2(D); the surfaces are mirror images of each other, as is the case also for Fig. 2(C).

B. Grand Canonical MC for confined fluids

In this section we present an overview of the formulation and implementation of the MC method (using the Metropolis algorithm [53]) in the Grand Canonical ensemble (at fixed chemical potential, volume and temperature) for the DPD model (GCMC-DPD) to simulate fluids confined by structured surfaces, at the mesoscopic scale. This methodology has been applied successfully by one of us (AGG) to study polymers, polyelectrolytes and colloids, among other systems. Readers can consult full details of the method in the original articles [54-56].

The confined fluid must be in chemical equilibrium with a reservoir at fixed chemical potential. Under this situation, one can model a fluid confined by rough surfaces, where the number of particles of the solvent has to be allowed to fluctuate. This is done by fixing the chemical potential of the solvent in the simulation. The Grand Canonical conditions can be readily included in a DPD simulation by performing creation/deletion of particles in a MC run. The algorithm attempts to create or delete a solvent particle with equal probability a number of times, using the GCMC acceptances rules [51]. However, when an inhomogeneous fluid is confined by walls, the rules for the creation and destruction of particles must be modified as a result of the confinement of the particles. Therefore, the probabilities for insertion and deletion of a particle are given by the following equations, respectively:

$$P_{\text{insertion}} = \min\left[1, \frac{\langle Z(z)\rangle V}{N+1} \exp\left(-\frac{\Delta U^{\text{test}}}{k_B \text{T}}\right)\right] \quad , \tag{4}$$

$$P_{\text{deletion}} = \min\left[1, \frac{N}{\langle Z(z)\rangle V} \exp\left(-\frac{\Delta U^{\text{test}}}{k_B \text{T}}\right)\right] \quad , \tag{5}$$

where ΔU^{test} is the total conservative interaction energy difference between the added or removed bead, and the N or $N-1$ remaining beads, respectively, including the conservative

interaction with the surface. $\langle Z(z) \rangle$ is the so-called activity, defined for inhomogeneous systems as [56]:

$$\langle Z(z) \rangle = \frac{\langle \rho(z) \rangle_{NVT}}{\left\langle \exp\left(-\frac{\Delta U^{\text{test}}}{k_B T}\right) \right\rangle_{NVT}} = e^{\frac{\langle \mu(z) \rangle}{k_B T}} \quad , \tag{6}$$

In eq. 6, $\mu(z)$ is the chemical potential for an inhomogeneous system in the z-direction, and the angular brackets represent averages in the NVT (canonical) ensemble. The total average z-dependent density is $\rho(z)$. The velocity of the inserted particle is chosen randomly using a Maxwell-Boltzmann distribution using the imposed temperature.

C. Interfacial properties for confined fluids

The combination of surface geometry and interfacial tension in the system may create new stable or metastable structures such as capillary bridges [57], and the presence of the confining walls may cause phase transitions to occur not seen in the bulk [58]. For this reason, the analysis of fluids confined in this work is based on the calculation of the profiles of various thermodynamic properties such as density, temperature, pressure, and interfacial temperature. The expressions for calculating the pressure profiles for confined fluids are slightly different from those commonly used for unconfined fluids. In this work, the confinement is applied along the z-direction of the simulation cell, where there is a variation of the particle local density along this direction, which produces an asymmetry in the pressure tensor. Thus, the pressure tensor, **P**, has two different z-dependent components, $P_N(z) = P_{zz}(z)$ and $P_T(z) = (P_{xx} + P_{yy}) / 2$, which are the normal and tangential components of the pressure tensor, respectively. Because the fluid's confinement appears only in the $z -$ direction, only P_N component must be modified, while the

component P_T remains unchanged with respect to a bulk (unconfined) fluid. Thus, $P_N(z)$ has two contributions, namely

$$P_N(z) = P_N^f(z) + P_N^W(z) \quad ,$$
(7)

where $P_N^f(z)$ and $P_N^W(z)$ are the contributions to the normal pressure component arising from the fluid (f), and from the walls (W), respectively. Following the Irving-Kirkwood definition [59] of the pressure tensor, the first term, $P_N^f(z)$, in eq. 7 can be rewritten for confined fluids as follows [60]:

$$P_N^f(z) = \frac{1}{V} \langle \sum_{i=1}^{N} m_i (v_i)_z (v_i)_z \rangle + \frac{1}{A} \langle \sum_{i}^{N} \sum_{i<j}^{N} (z_{ij})(F_{ij})_z \frac{1}{|z_{ij}|} \theta\left(\frac{z-z_i}{z_{ij}}\right) \theta\left(\frac{z_j-z}{z_{ij}}\right) \rangle ,$$
(8)

where N is the total number of particles, $V = A\Delta z$ is the volume of a slab of the simulation box of thickness Δz and transversal surface area $A = LzLy$, m_i is atomic mass of the fluid particles, $(v_i)_z$ is the velocity in the z direction of the ith particle, $(F_{ij})z$ is the z-component of the total conservative force between particles i and j, $\theta\left(\frac{z-z_i}{z_{ij}}\right)$ is the unit step function which is equal to 1 when $\left(\frac{z-z_i}{z_{ij}}\right) > 0$ and zero otherwise, and z_{ij} is the distance between the particle i and j in the z direction. The tangential component, $P_T^f(z)$, can be obtained by replacing z_{ij} by $\sqrt{\frac{1}{2}(x_{ij}^2 + y_{ij}^2)}$ in eq. 8. The second term, $P_N^W(z)$, in eq. 7 describes the contribution of the walls to the normal pressure. This contribution is given by $P_N^W(z) = P_N^{W_1}(z) + P_N^{W_2}(z)$, where $P_N^{W_1}(z)$ and $P_N^{W_2}(z)$

are the normal pressure components of the surfaces evaluated at the positions $z_{W_1} = 0$ and

$z_{W_2} = L_z$, respectively. The contribution of the first surface, $P_N^{W_1}(z)$, is given by

$$P_N^{W_1}(z) = -\frac{1}{A} \langle \sum_i^N (z_i^{W_1})(F_i^{W_1}) \theta \left(\frac{z_i - z}{z_i^{W_1}} \right) \theta \left(\frac{z - z_{W_1}}{z_i^{W_1}} \right) \rangle , \tag{9}$$

where $z_i^{W_1}$ and z_i are the positions both of the first wall and the ith particle in the z direction;

$F_i^{W_1}$ is the conservative force between the fluid and the first surface. Analogously, one can write

the expression for the contribution to the normal pressure arising from the second wall, $P_N^{W_2}(z)$

as follows:

$$P_N^{W_2}(z) = -\frac{1}{A} \langle \sum_i^N (z_i^{W_2})(F_i^{W_2}) \theta \left(\frac{z_{W_2} - z}{z_i^{W_2}} \right) \theta \left(\frac{z - z_i}{z_i^{W_2}} \right) \rangle . \tag{10}$$

In this case, $z_i^{W_2}$ and z_i correspond to the positions of the second wall and the ith particle in the z

direction, respectively; $F_i^{W_2}$ is the conservative wall force between the fluid and the second

surface. The forces, $F_i^{W_1}$ and $F_i^{W_2}$ in eqs. 9 and 10, respectively, are both given by eq. 3. The

interfacial tension profile, $\gamma(z')$, for fluid-fluid and fluid-wall interfaces is obtained in terms of

normal and tangential pressures using the following expression:

$$\gamma(z') = \int_0^{L_z'} [P_N(z) - P_T(z)] dz . \tag{11}$$

All the methodology described in this work has been implemented in our simulation code, called SIMES, which is designed to study complex systems at the mesoscopic scale using graphics processors technology (GPUs) [61].

III. SIMULATION DETAILS

Four different models of confined fluids were analyzed, namely those confined between smooth surfaces (SS); surfaces with symmetric roughness (RR), surfaces with non – symmetric roughness (AA), and a combination between a smooth surface and a surface with symmetric roughness (SR). Our simulations were performed using reduced units so the all masses are equal to one, as are the cutoff distances r_c and z_c. The values that define the dissipative and random force intensities are $\gamma = 4.5$ and $\sigma = 3.0$, so that $k_B T^* = 1$ for all simulations. Furthermore, the conservative force intensities for the fluid were chosen as $a_{ij} = 78$ units, which correspond to a coarse-graining degree of 3 water molecules grouped into a DPD bead [47]; from it one can extract a dimensionalized value for $r_c = 6.46$ Å, which is the characteristic length scale for our simulations. On the other hand, the repulsive wall – fluid interaction parameter, a_{w-ie} (eq. 2), was chosen as $a_{w-ie} = 140$ units in all simulations. Higher values of this parameter lead to very repulsive walls, while very small values lead to attractive and soft walls. The chemical potential chosen for the solvent so that the average density obtained was of $\langle \rho^* \rangle = 3.0$ was set at $\mu^* = 37.7$. By choosing this average density, one has the smallest system where the DPD quadratic equation of state obeys the scaling law that makes it independent of the choice of particle-particle interaction parameters [45]. The properties were calculated with simulations of at least 50 blocks, of 5×10^4 MC configurations each one, with the first 10 blocks used to equilibrate the system; the percentage of successful MC moves was between 35-40 %. The dimensions of the simulations box were $L_x = L_y = L_z = 10.0$ for the all simulations, and periodic boundary conditions

were used, except in the *z*-direction since this is the direction of the confinement. The time step

chosen for the dynamics part of the simulation was set to $\delta t^* = 0.001$, and the DPD beads were

moved using the velocity Verlet algorithm [62]. This value of δt^* allows us to maintain an

acceptance rate of between 35% and 40%. To evaluate the density, pressure, temperature and

interfacial tension profiles, the *z*-length of the simulation box, L_z, was divided into N_s slabs of

width $\Delta z = 0.005$ units. These profiles were calculated as

$$\langle X(Z) \rangle = \frac{\langle X(\Delta N) \rangle}{\Delta V} \,, \tag{12}$$

Where X refers to the density (ρ), pressure (P), temperature (T) or interfacial tension (γ),

$\langle X(\Delta N) \rangle$ is the average of X as a function of the number of particles with coordinates between z

and $z + \Delta z$, $\Delta V = L_z L_y \Delta z$ is the volume of the slab. The effect of the roughness of the walls in our

simulations is controlled by the a_R and λ_1 parameters, see eq. 3. We analyze the behavior of

these parameters in two sets of simulations. In the first set of simulations λ_1 remains constant, λ_1

$= \pi$, $\lambda_2 = 0$, with different values of a_R namely, $a_R = 0.0$, 0.5, 1.0. In the second set of

simulations a_R is constant, ($a_R = 1.0$) while λ_1 takes the values of $\pi/4$, π, $7\pi/4$. Only for

asymmetrical walls is $\lambda_2 \neq 0$.

IV. RESULTS AND DISCUSSION
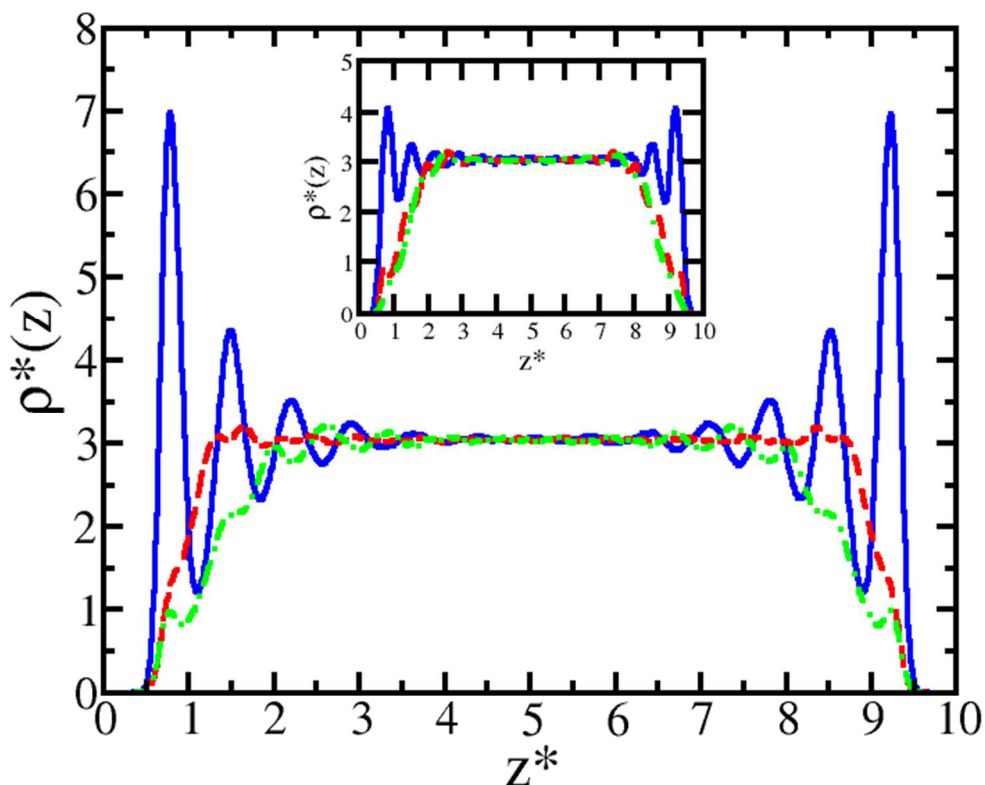
Figure 3. (Color online) Density profiles of the fluid as a function of the magnitude of the surfaces roughness. The degree of confinement is analyzed in the z – direction of the simulation cell, namely perpendicularly to the walls. The main panel in the figure shows the effect of varying the magnitude of the parameter a_R, see eq. 7. These profiles were obtained at fixed $\lambda_1 = \pi$, for different values of a_R: $a_R = 0.0$ (solid line), $a_R = 0.5$ (dashed line), and $a_R = 1.0$ (dashed – dotted line). The density profiles with a_R constant ($a_R = 1.0$) while varying λ_1, are presented in the inset, with $\lambda_1 = \pi/4$ (solid line), $\lambda_1 = \pi$ (dashed line), and $\lambda_1 = 7\pi/4$ (dashed - dotted line). The type of surface generated with the parameters $\lambda_1 = \pi$ and $a_R = 1$ is defined in Table I, i.e., both surfaces are symmetrically structured walls; see also Fig. 2(C). In all cases $\lambda_2 = 0$. The axes are shown in reduced DPD units.

Let us start by considering the influence of two symmetrically structured walls (see Fig. 2(C)) on a simple fluid. In Fig. 3 we show the density profiles obtained for these surfaces when the amplitude of the structure (a_R, main panel) and the periodicity of it (λ_1, inset) are changed. The case of two planar walls (Fig. 2(A)) is included also, which corresponds to $a_R = 0$. The fluid is structured the most when the walls are flat (solid line in the main panel in Fig. 3), which is to be expected, because the fluid particles can order more easily into layers, giving rise to the peaks in the figure [63]. Another relevant aspect is that the periodicity of the structure induced in the fluid

(see solid line in Fig. 3) is approximately equal to the diameter of the molecules that make up the fluid; this is also known using other methods and experiments [63]. As the amplitude of the structure is increased (a_R), the structure in the fluid tends to disappear rather quickly, reaching the bulk (unconfined) density, which occurs because the fluid's particles cannot easily arrange themselves into layers. The effect of the periodicity of the structure (λ_1) seems to play a secondary role, as seen in the inset in Fig. 3, where the structure in the fluid is barely apparent. The results shown in Fig. 3 demonstrate that the first few layers of the fluid's particles adjacent to the walls reflect the symmetry of the walls that confine them, and since they are structured (except when $a_R = 0$) the formation of layers is unfavorable. The density profiles along one of the sides of the walls confirm this assertion, as shown in Fig. 4. Wettability is maximum for the planar wall (solid line in main panel of Fig. 3), as expected, and is reduced as the roughness of the structured walls is increased, when $\lambda_1 = \pi$. When the amplitude of the wall's roughness if fixed, $a_R = 1.0$, the maximum wettability is obtained for $\lambda_1 = \pi/4$, see the inset in Fig. 3, because the structure on the walls is smaller than the size of the fluid particles, therefore this structured wall is similar to the smooth wall.
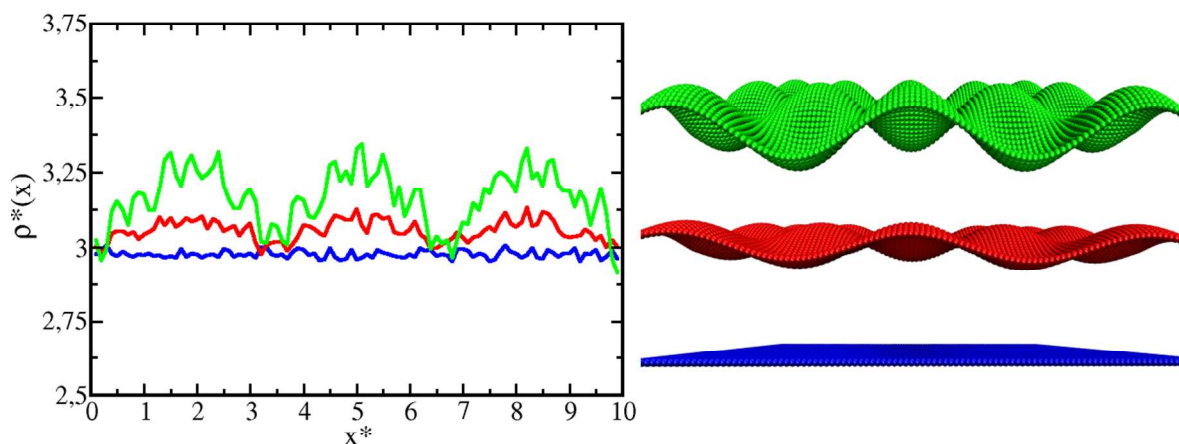
Figure 4. (Color online). Left. Density profiles in the x – direction for different values of the parameters of roughness. These profiles were obtained at fixed $\lambda_1=\pi$, for different values of a_R: $a_R = 0.0$ (blue line), $a_R = 0.5$ (red line), and $a_R = 1.0$ (green line); in all cases, $\lambda_2 = 0$. The axes are shown in reduced DPD units. Right. Schematic representation of the different morphologies of the surfaces shown in the density profiles.

Figure 4 shows the density profiles of the fluid on plane of the structured surfaces, specifically in the x – direction, showing clearly how the fluid follows the symmetry of the substrate increasingly as the structure becomes more pronounced. The maxima seen in the left panel in Fig. 4 correspond to maxima in the images shown in the right panel. Equivalent density profiles are obtained in the y–direction, of course, but they do not add new information to that given by Fig. 4, therefore they are not presented. It is important to notice that the periodicity seen in Fig. 4 is not at all related to the size of the fluid's molecules, as for the smooth surfaces case in Fig. 3. This results from the fact that the fluid is not bound in the x – direction, since periodic boundary conditions were used there. However, the structure seen in the density profile shown in the left image in Fig. 4 is due solely to the symmetry of the structured walls.

Although the structure of the walls can be significant on the scale of the simulation box, see for example, the green structure on the right panel of Fig. 4, the system is always in thermal equilibrium. This can be ascertained from inspection of Fig. 5, which is the temperature profile

of the fluid along the direction perpendicular to the plane of the walls; the temperature of the

fluid remains constant and equal to the value imposed by the thermostat, i.e. $k_B T^* = 1$, regardless

of the structure on the surfaces confining the fluid. Neither the amplitude of the structure (main

panel in Fig. 5), which determines the strength of the surface – fluid interaction, nor the

periodicity of it perturb the temperature of the fluid, once equilibrium has been achieved, as

should be expected.
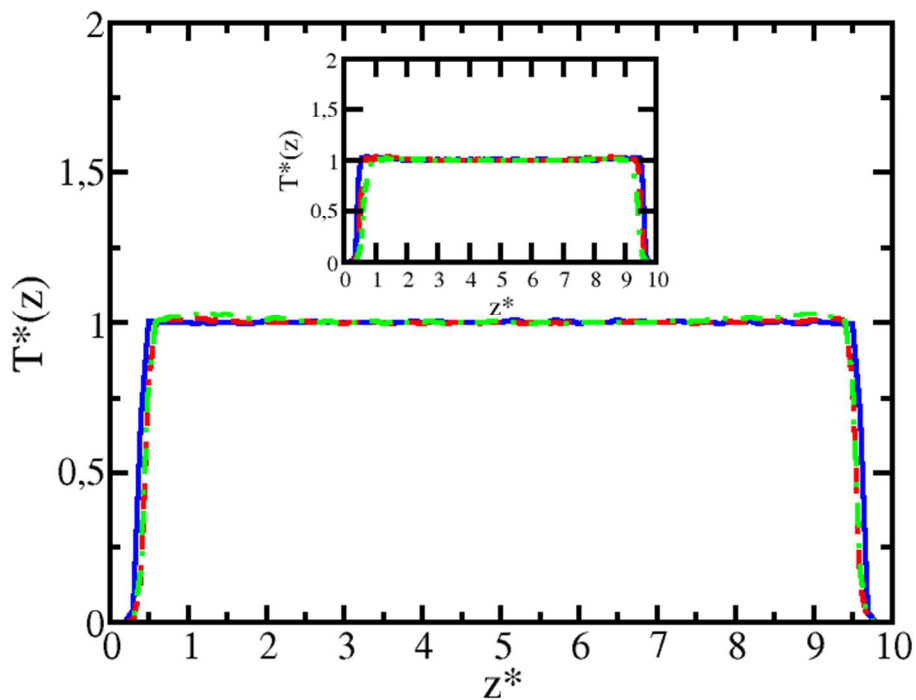
Figure 5. (Color online) Temperature profiles of the fluid particles along the z – direction. In the main panel, λ_1 remains constant ($\lambda_1=\pi$), for different values of a_R. The a_R values are the same as those presented in Fig. 3. The temperature profiles at fixed $a_R = 1.0$ while varying λ_1 are presented in the inset, with the same λ_1 values as those presented in Fig. 3. The color code of the lines is the same as in Fig. 3. The axes are shown in reduced DPD units.
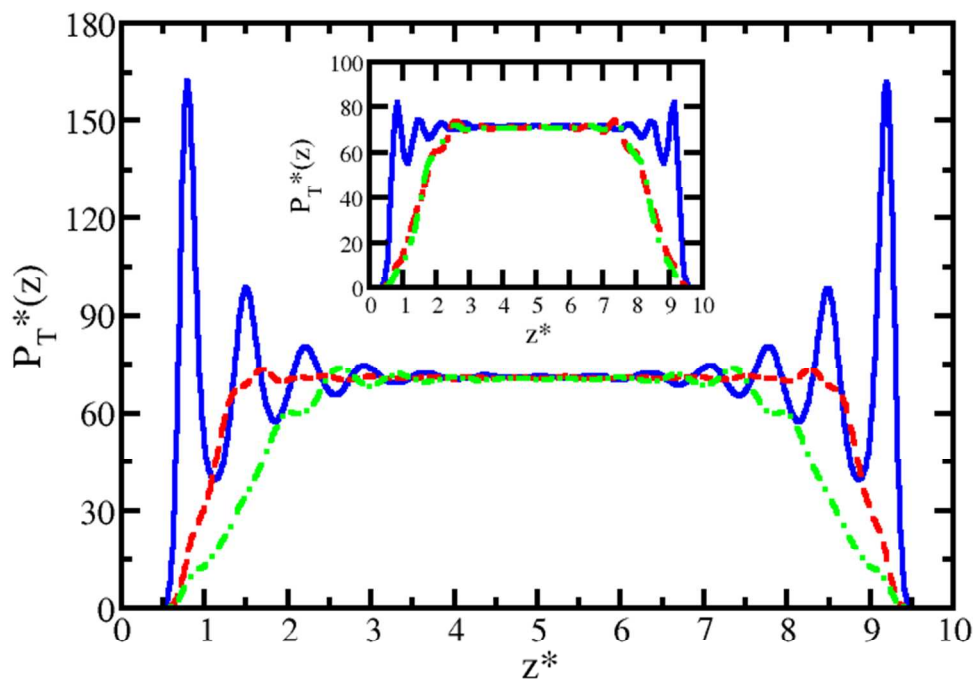
Figure 6. (Color online) Tangential pressure (P_T) profiles of a fluid confined by smooth and rough surfaces. These profiles were obtained at constant $\lambda_1=\pi$, for different values of a_R, namely, $a_R = 0.0$ (solid line), $a_R = 0.5$ (dashed line), and $a_R = 1.0$ (dashed – dotted line). The profiles of the tangential pressure with a_R constant while varying λ_1 are presented in the inset; in this case $a_R = 1.0$, with $\lambda_1=\pi/4$ (solid line), $\lambda_1= \pi$ (dashed line), and $\lambda_1=7\pi/4$ (dashed dotted line). See eq. 3. The axes are shown in reduced DPD units.

In Fig. 6 we show the tangential pressure profiles of the fluid along the z – direction. Only for the smooth, planar surface (see Fig. 2(A)) do the fluid molecules display significant layering (solid line in the main panel of Fig. 6), while as the amplitude of the wall structure is increased, such layering disappears, in agreement with the trends found for the corresponding density profiles (Fig. 3). For the smooth surfaces, the layering in the tangential pressure profile has periodicity approximately equal to one molecular diameter, just as in the density profile (Fig. 3) because of the confinement in z – direction [63]. The influence of the periodicity of the walls in the tangential pressure profiles is the same as that found in the density profiles, as seen in the inset of Fig. 6 in comparison with the inset of Fig. 3.
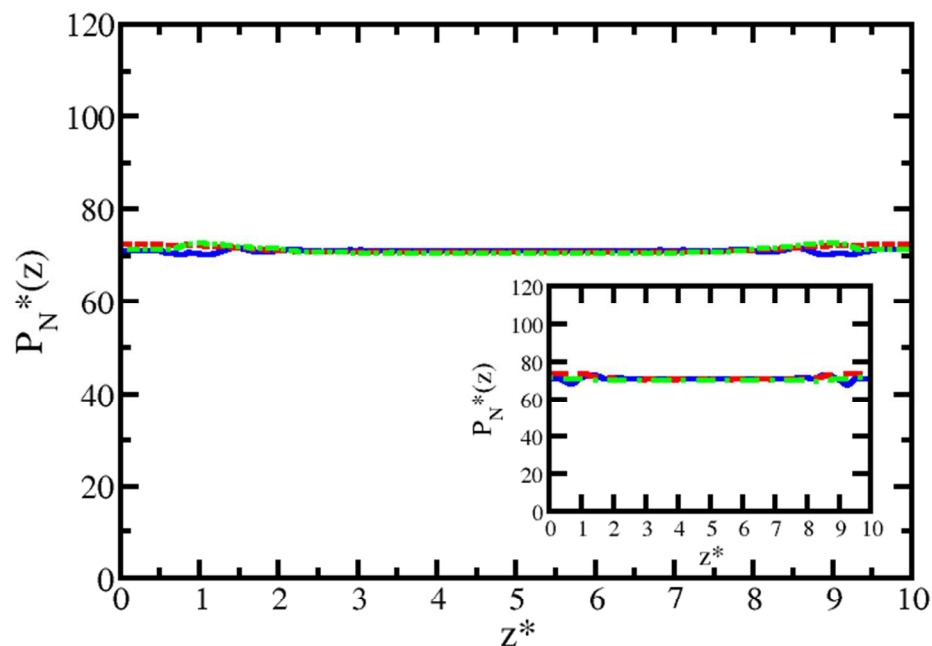
Figure 7. (Color online) Profiles of the component of the pressure tensor normal to the surfaces as functions of the parameters of roughness. These profiles were obtained at fixed $\lambda_1=\pi$, for different values of a_R: $a_R = 0.0$ (solid line), $a_R = 0.5$ (dashed line), and $a_R = 1.0$ (dotted line). The profiles of the normal pressure component at constant a_R while varying λ_1, are presented in the inset, for $a_R = 1.0$, and $\lambda_1=\pi/4$ (solid line), $\lambda_1= \pi$ (dashed line), and $\lambda_1=7\pi/4$ (dashed dotted line). The axes are shown in reduced DPD units.

The mechanical equilibrium of the fluid confined by structured surfaces is clearly seen by the constant profile of the component of the pressure tensor normal to the surfaces, P_N, shown in Fig. 7. Even for the most structured walls, the normal pressure remains constant, as expected. Its value is somewhat larger than the value of the tangential pressure away from the walls, which is a consequence of the finite interfacial tension between the fluid and the surfaces. This is quantitatively evaluated using eq. 11, and is presented in Fig. 8. Interestingly, the value of the pressure normal to the walls does not depend on the solid – fluid interaction either, as the main panel in Fig. 7 shows. Once the fluid is confined, such component of the pressure tensor depends only on the interactions between the molecules of the fluid [53]. The solvation force depends, of

course, on the confinement degree also and has been shown to display exponentially decaying

oscillations for simple fluids [65-66], but those aspects are the result of the confinement only and

are predominant for smooth surfaces, which are not the focus of this work.
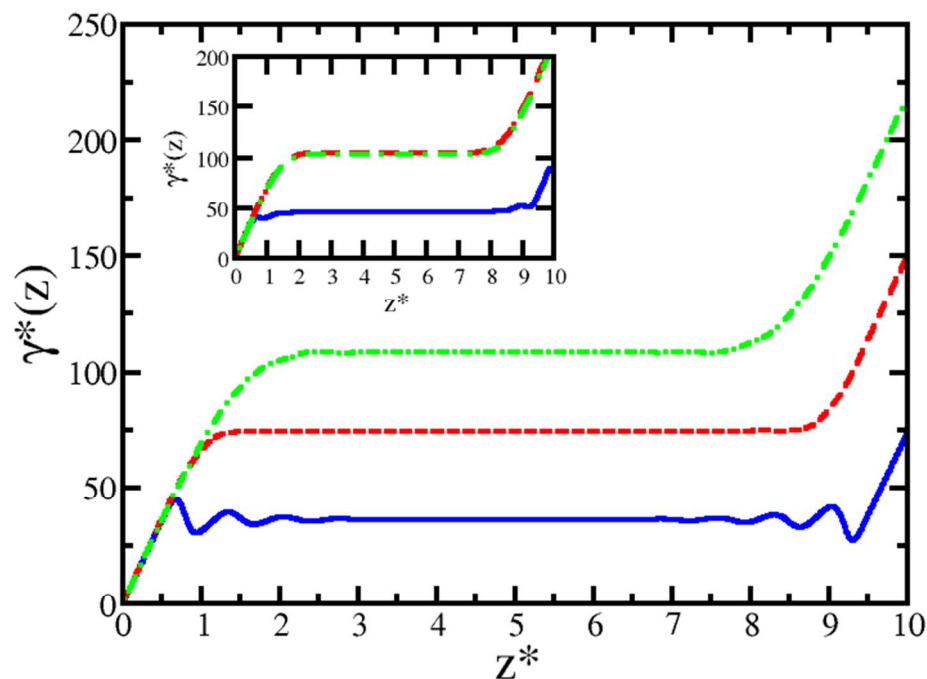
Figure 8. (Color online) Interfacial tension profiles for different values of the parameters of the walls' roughness. In the main panel, λ_1 remains constant ($\lambda_1=\pi$), for different values of a_R; the a_R values are 0 (solid blue line), 0.5 (dashed red line), and 1.0 (dashed –dotted green line). The profiles of interfacial tension with a_R constant ($a_R = 1.0$) while varying λ_1 are presented in the inset; the λ_1 values are $\lambda_1=\pi/4$ (solid line), $\lambda_1= \pi$ (dashed line), and $\lambda_1=7\pi/4$ (dashed dotted line). The axes are shown in reduced DPD units.

The interfacial tension profiles shown in Fig. 8 are symmetric because the surfaces that confine

the fluid are also symmetrically structured. The oscillations close to the walls that can be seen in

the solid line in Fig. 8 correspond to the smooth walls and are once again the consequence of the

ability of the fluid to form more or less well ordered layers close to the surfaces. However, as the

amplitude of the structuring is increased the oscillations disappear but the value of the interfacial

tension grows monotonically with the parameter a_R (see eq. 3). The influence of the periodicity

of the structure on the walls seems to be a secondary effect, as the inset in Fig. 8 shows, where the lowest interfacial tension profile is obtained for the structure with the smallest periodicity ($\lambda_1 = \pi/4$, see eq. 3). This occurs because the diameter of the fluid particles is larger than such periodicity, therefore they tend to organize themselves into ordered layers, which lowers the interfacial tension. This feature can be understood also by inspection of the tangential pressure profiles shown in the inset of Fig. 6, where the largest profile corresponds to the case with the wall periodicity equal to $\lambda_1 = \pi/4$; hence, its corresponding value of γ must be the smallest, see eq. 11, as is indeed the case seen in the inset of Fig. 8. Equivalently, the tangential pressure profiles for $\lambda_1 = \pi$ and $\lambda_1 = 7\pi/4$ (inset in Fig. 6) are almost indistinguishable, as are their normal pressure counterparts (inset in Fig. 7), which in turn leads to indistinguishable interfacial tension profiles (inset in Fig. 8). One notices also that the cases with maximum wettability (see discussion of Fig. 3) correspond to cases with the lowest interfacial tension, see the solid lines in the main panel and inset in Fig. 8; these are the expected results.

The layering of a confined fluid occurs even when there are no interactions between the fluid's particles, as in a hard – sphere liquid, or even when there is no attraction between the walls and the fluid [63]. The strength of the fluid – fluid interactions with respect to the wall – fluid interaction can, of course, increase the layering of the fluid, and hence the resulting interfacial tension. However, in the present study we have chosen to keep those interactions constant ($a_{ij} = 78$, $a_{i\_w} = 140$) and focus instead on the influence of the structure of the confining surfaces on the layering of the fluid and on the interfacial tension. Moreover, there are reports in the literature that have studied the influence of the fluid – wall interaction on the structuring of confined fluids [67] for smooth walls, therefore it is befitting to explore the consequences of structured walls on thermodynamic properties such as the interfacial tension.
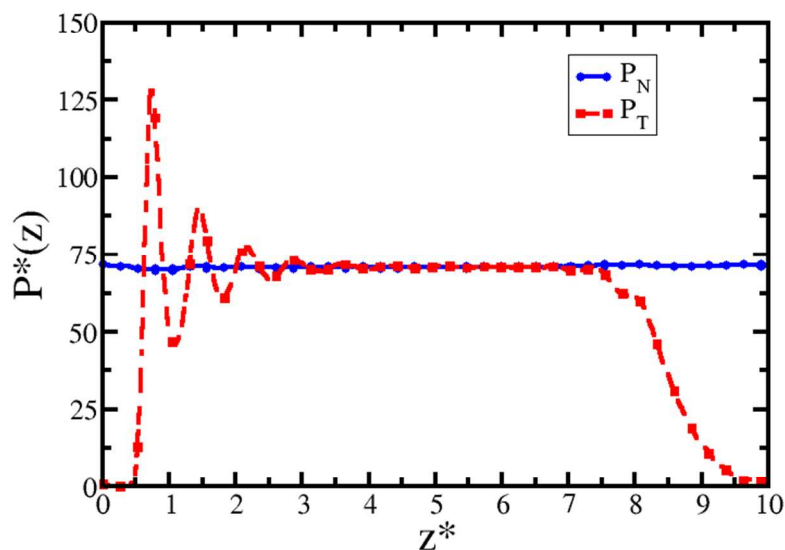
Figure 9. (Color online) Pressure tensor components for the fluid confined by a smooth surface on the left of the simulation cell ($z^* = 0$), and a rough surface on the right of the simulation cell ($z^* = 10$). See image (B) in Fig. 2. The filled circles connected by a solid line represent the normal pressure while the filled squares connected by a dashed line are the tangential pressure. The axes are shown in reduced DPD units. The geometric parameters for the rough surface shown in this case are $\lambda_1 = \pi$ and $a_R = 1.0$.

Let us now consider the case when the fluid is confined by differently structured walls. In Fig. 9 we present the pressure profiles for a fluid flanked on the left by a featureless, smooth wall and on the right by a symmetrically structured surface. The normal pressure profiles is constant, as expected for a confined fluid in equilibrium, but the tangential pressure profile is asymmetric, showing strong structuring near the smooth wall ($z^*=0$ in Fig. 9), where the fluid particles have complete freedom to arrange themselves into ordered layers, that extend up to about $z^*=3$. One then should expect a relatively low value of the interfacial tension at the left interface. The situation for the interface on the right ($z^*=10$ in Fig. 9) is entirely different, because the structure on the wall "washes out" all the possible ordering of the fluid into layers, producing only a reduction of the tangential pressure. As eq. 11 indicates, one should expect here a larger value of the interfacial tension than that on the left interface. This is precisely what is found, as shown in

Fig. 10, where the interfacial tension profile for the system whose pressure profiles are shown in Fig. 9 is calculated. Some oscillations appear in the interfacial tension close to the smooth wall (on the left), which are inherited from the oscillations in the tangential pressure profile (filled squares in Fig. 9).
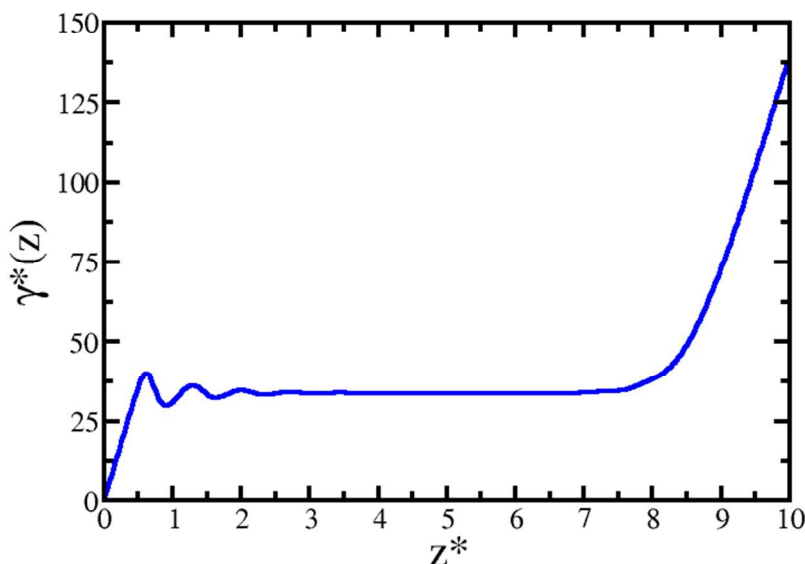
Figure 10. Interfacial tension profile of the fluid confined by the surfaces whose pressure profiles are shown in Fig. 9. On the left of the simulation box (z*=0) there is a smooth wall, while a highly structured surface is placed on the right, with parameters $\lambda_l=\pi$ and $a_R = 1.0$. The axes are shown in reduced DPD units.

Notice that the perturbations introduced into the interfacial tension profile, i. e. the regions where this profile is not constant, have the same extent into the $z-$ direction; in the case shown in Fig. 10 these regions comprise a thickness of about z* = 3.0 on each wall. However, the amplitude of the structure on the rough wall does influence greatly the value of the interfacial tension: while the smooth wall raises the interfacial tension up to γ* = 30 (on the left in Fig. 10), the structured wall raises it up to γ* = 137. This amplitude depends on the nature of the solid that makes up the surfaces, and on the properties of the confined fluid [63].
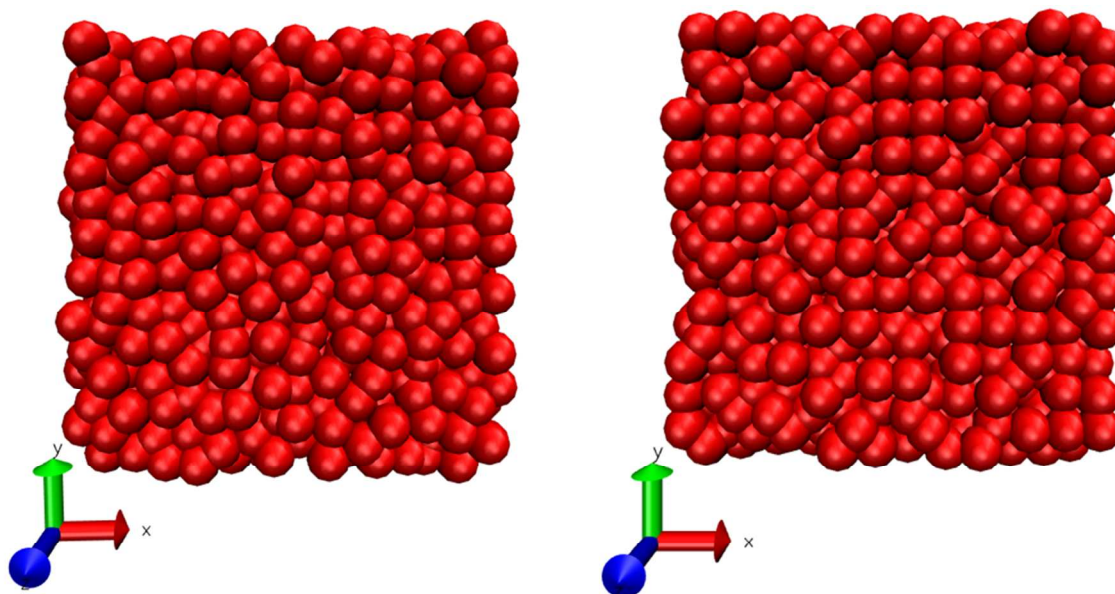
Figure 11. Snapshots of a face of the simulation box on the xy - plane in equilibrium for model B in Fig. 2. Left, the arrangement of the first layer of particles on a smooth surface (bottom surface in Fig 2B). Right, the arrangement of the first layer of particles on a symmetrically structured surface (top surface in Fig 2B). Notice how some particles display an almost crystalline arrangement near the structured wall (right image). The structural parameters for the latter are: $\lambda_1 = \pi$ and $a_R = 1.0$. These images were obtained with VMD [52].

The snapshots of the left and right faces of the simulation box whose interfacial tension profile was presented in Fig. 10 are shown in Fig. 11, with the purpose of clarifying why there are oscillations in that profile for a smooth surface (left image in Fig. 11) and why they are absent when the wall is structured (right image in Fig, 11). When the surface is smooth, as in the left image in Fig. 11, particles can form layers more easily parallel to the xy – plane, as this increases their translational entropy. Those layers, which are made of particles with full symmetry (disordered) on the xy – plane, induce ordering along the z – axis, which is responsible for the oscillations seen in density profiles (see left side of Fig. 3), tangential pressure profiles (see Fig. 6) and interfacial tension profiles (see Figs. 8-10). On the order hand, when there is a structured surface, as in the right image in Fig. 11, particles have reduced symmetry (ordered) on the xy –

plane, and they form pockets with quasi-crystalline order (right image in Fig. 11), which produces full symmetry (disorder) along the $z-$ axis. These two contrasting cases are present in Fig. 3, namely when there is full symmetry (disorder) on the $xy-$ plane (solid line, a_R=1.0), the fluid forms layers (order) along the $z-$ direction. However, when the surfaces impose their order on the $xy-$ plane to the fluid particles ($a_R = 1.0$, $\lambda_1 = \pi$, dashed $-$ dotted line), there appears disorder along the $z-$ axis. This order $-$ disorder phase transition has been studied in molecularly thin confined films [64], but it has never been investigated in mesoscale –structured pores to the best of our knowledge.

It is also of interest to find out how the thermodynamic and structural properties of pores behave when both confining surfaces are symmetrically structured (as in Fig. 2C), as compared with the case when both walls are asymmetrically structured (as in Fig. 2D). In Fig. 12 we compare the interfacial tension profiles of these two cases, finding that they are the same regardless of the symmetry or asymmetry of the walls, as long as a_R remains the same in both cases. The insets in Fig. 12 show that the normal pressure profiles and the density profiles are also the same for the fluid confined by symmetrically and asymmetrically structured surfaces. Mechanical equilibrium is maintained in both cases, as seen by the constant normal pressure profiles (lower right inset in Fig. 12), as expected. What is somewhat more surprising is that the particles of the fluid adsorb in a disorderly fashion over both types of confinement, as seen in the upper left inset in Fig. 12. The ordering on the $xy-$ plane induced by symmetric and asymmetric walls prevents the fluid molecules from ordering along the $z-$ direction, which leads to almost identical interfacial tension profiles. The most important factor regarding the value of the interfacial tension is the value of the interaction between the solid surfaces and the fluid molecules, a_R, which is the same for all the cases shown in Fig. 12.
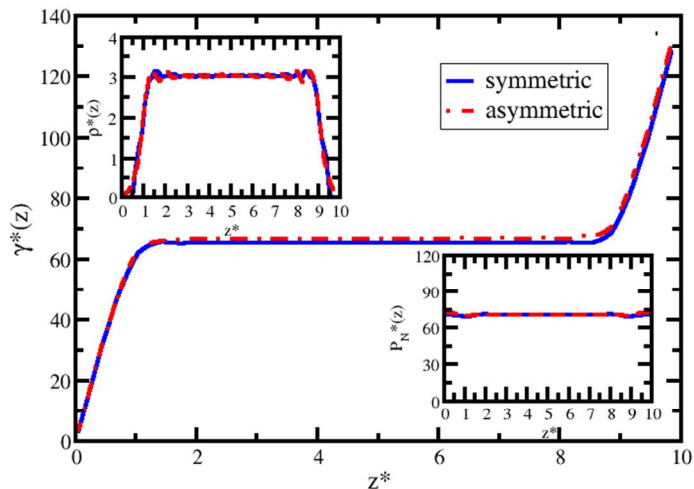
Figure 12. (Color online). Interfacial tension, density, and pressure profiles for symmetrically and asymmetrically structured walls. The symmetrically structured walls shown in this figure correspond to model C in Fig. 2, whose geometrical parameters are $\lambda_1=\pi$ and $a_R = 0.5$. The asymmetrically structured walls shown in this figure correspond to model D in Fig. 2, whose geometrical parameters are $\lambda_1=\pi$, $\lambda_2=0.1$ and $a_R = 0.5$, see eq 3. The solid line (blue line) is the profile for symmetric walls, while the dotted line (red line) is the profile for asymmetrical walls. The main panel shows the interfacial tension profiles. The inset in the upper left corner shows the density profiles for each case shown in the main figure, and the inset in the lower right corner shows the pressure profiles for the symmetrically and asymmetrically cases.

To determine the extent to which the structure of the solid induces stratification in the liquid can be evaluated with the spatial evolution of the two – dimensional (xy – plane) radial distribution function as one samples the correlation between fluid particles away from the surface of the solid, see Fig. 13.
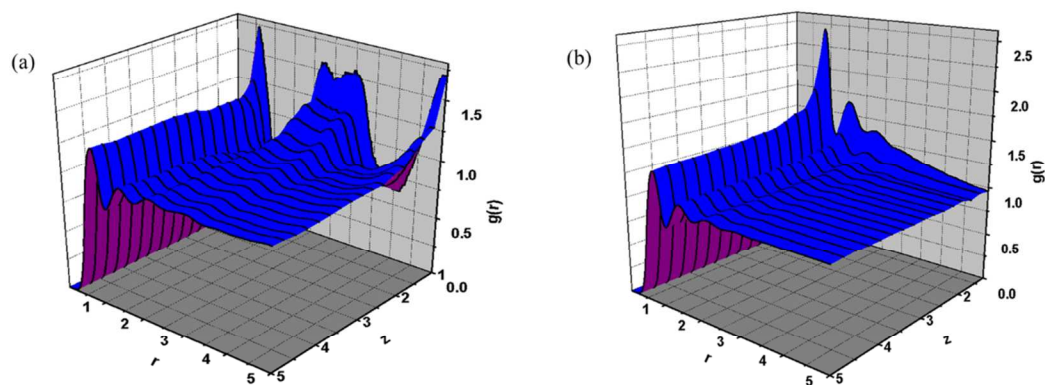
Figure 13. Three – dimensional evolution of the radial distribution function of a fluid confined by symmetrically structured walls, as in Fig. 2 C. These cases correspond to roughness parameters equal to (a) $\lambda_1=\pi$, and $a_R = 1.0$; (b) $\lambda_1=6\pi$, and $a_R = 1.0$. The distance r is the correlation distance on the xy – plane.

As Fig. 13 shows, the fluid layer in contact with the structured surface is also highly structured ($z=0$ in Fig. 13), but as the distance along the z – axis is increased with respect to the surfaces, the correlations in the fluid tend to disappear, becoming almost bulk – like at the largest distances ($z=5$ in Fig. 13). Even for a solid – like ordering of the fluid particles close to a structured wall, see Fig. 13 (a) and the snapshot on the right in Fig. 11, such ordering disappears if the simulation box is large enough so that the fluid is allowed to regain its full symmetry. When the periodicity of the structure on the surface is very large, as is the case shown in Fig. 13 (b), the wall appears almost as a smooth surface to the fluid particles closest to it, and the transition order – disorder occurs at smaller distances from the wall. Lastly, one notices that the period of the oscillations of the radial distribution functions changes from being given by the structure of the walls, when z=0, to becoming approximately equal to the diameter of fluid's molecules, which is the intrinsic feature of the radial distribution function of a fully homogenous and isotropic fluid.

As a final assessment of the order – disorder transition in smooth and structured surfaces, we have calculated the profile of the order parameter, S, defined as $S = 3\langle cos^2\theta \rangle - 1/2$ [49], where θ is the angle formed by the unit vector in the z – direction with the vector $\vec{r}_{ij} = \vec{r}_i - \vec{r}_j$. The results are presented in Fig. 14; the solid line, which corresponds to smooth walls, shows the most ordering close to the surfaces. There appear peaks with the same periodicity as those in the density, pressure and interfacial tension profiles, which is roughly the size of the fluid particles [68]. The structured surface whose periodicity on the xy – plane is smaller than the size of the fluid's particles, $\lambda_1 = \pi/4$, shows also strong ordering near the walls along the z - direction

(dashed line in Fig. 14). These two cases correspond to those of maximum wettability and order along the z – axis, coupled with disorder on the xy – plane. The dotted line in Fig. 14 is the order parameter profile of a strongly structured wall with large periodicity ($a_R = 1.0, \lambda_1 = \pi/4$), which corresponds to a case of low wettability (see Fig. 3) and considerable ordering on the xy – plane (see Fig. 11). However, as is clearly seen in Fig. 14, this structure is disordered close to the surfaces, in comparison with the other two cases shown in the figure, confirming our analyses of the structural and thermodynamic properties of the systems studied in this work.
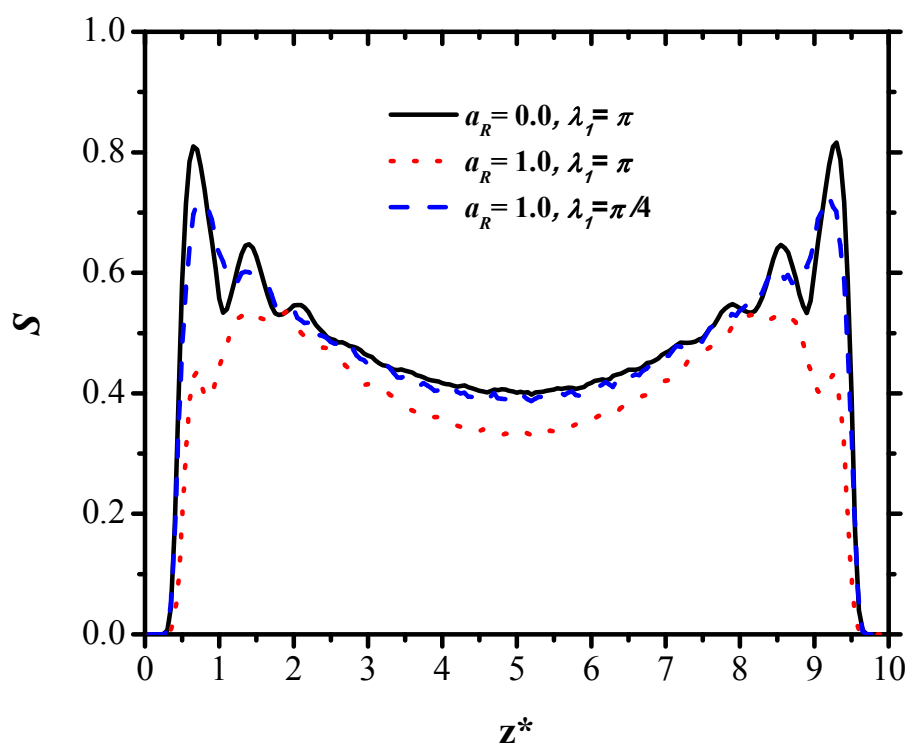
Figure 14. (Color online) Order parameter profiles showing ordered phases near the walls. The solid black line represents the profile of smooth surfaces, which shows the largest ordering near the walls. The blue dashed line is

32

the profile of the order parameter for surfaces with large structure amplitude ($a_R = 1$) but periodicity smaller than the size of the fluid's particles ($\lambda_1 = \pi/4$). The dotted line shows the profile for a strongly structured wall with large periodicity on the xy – plane ($a_R = 1, \lambda_1 = \pi$) where the fluid is relatively disordered along the z – direction. See text for details.

Although there are studies of the influence of structuring of the walls confining fluids on their thermodynamic properties [67, 69-70] at the atomistic level, ours is the first mesoscopic – level study we are aware of.

V. CONCLUSIONS

The thermodynamic and structural properties of a simple fluid confined by structured solid surfaces were studied here in detail using mesoscopic scale simulation techniques. It is found that when the fluid is confined by smooth walls it retains its homogeneity in the two dimensions where it is not bound, but its molecules order along the direction perpendicular to the confining surfaces. Structured surfaces induce ordering on the plane on which they bound the fluid, but disorder is found in the perpendicular direction. This phenomenon represents an order – disorder phase transition on a mesoscopic scale, which is a novel aspect of our work. We calculated interfacial tension profiles for several types of surfaces, and found that the most important factor in determining the value of the interfacial tension is not the geometry of the walls but the intensity of the solid wall – fluid interaction. The periodicity of the symmetry or lack thereof on the walls induces order or disorder on the fluid molecules adjacent to those walls, but plays a very minor role in the measurable value of the interfacial tension. These findings should be relevant for researchers working on the enhanced recovery of oil from complex pores and in microfluidics, among other nanotechnological applications.

Physical Chemistry Chemical Physics Accepted Manuscript

Appendix. Influence of the coarse – graining degree on structural properties of the confined fluid.

The effect of the coarse-graining degree on a DPD fluid confined by flat surfaces is presented here. The beads in DPD simulations are to be interpreted as a coarse graining of a fluid section rather than groups of the atoms or molecules. Because of this feature only structure and behavior that occur on length scales larger than the size of the beads have physical relevance. The coarse-graining can be taken in DPD simulations as [46]:

$$N_m = \frac{M}{m},\tag{A1}$$

where M is the mass of a bead DPD and m is the mass of a water molecule. When N_m is changed the conservative force constant, a, is also changed: $a = k_B T (\kappa^{-1} N_m - 1)/2\alpha\rho$, where κ is the reduced isothermal compressibility of water, α is a numerical constant equal to 0.101, and ρ is the density of the DPD fluid [45]. That is how the coarse – graining degree enters into the simulations operatively. We studied the effect of N_m on thermodynamic properties such as density and tangential profiles, the periodicity of the structure on the walls (see λ_l in eq. 3 in the

text), and radial distributions functions for flat surfaces. The analysis was performed for four different values of N_m, namely, $N_m = 1,2,3,4$. The details of the simulations presented in this Appendix are the same as those of the simulations presented in the manuscript. The only difference is that for cases presented in this Appendix we used a simulation cell with a volume equal to $L_x=L_y=L_z=12.0$, except where indicated otherwise.

In Fig. A1 we show the density profiles obtained for four different values of N_m when the DPD fluid is confined by smooth walls. As the coarse graining degree is increased, the amplitude of the layers closest to the wall is reduced, as should be expected since in the continuum limit the layers disappear. Notice also that the amplitude of the oscillations decays abruptly away from the wall, while the periodicity of those oscillations remains constant and approximately equal to the size of the DPD particles, r_c. This feature is in agreement with the Fisher – Widom conjecture [68] for the decay of correlations in systems under the influence of repulsive, short – range potentials, such as the DPD interaction.
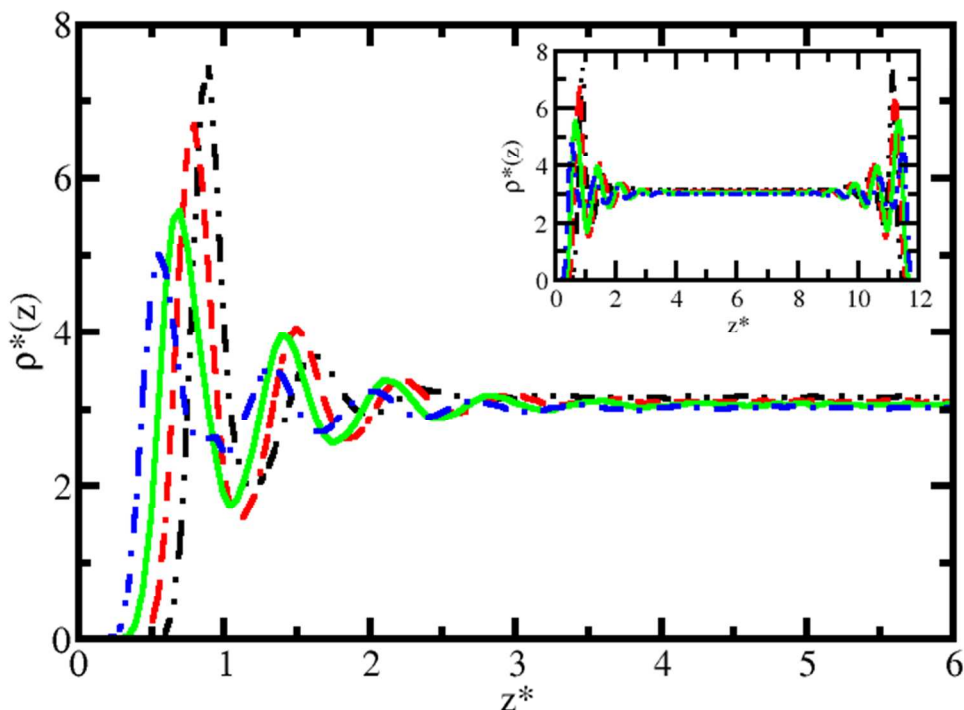
Figure A1. (Color online) Influence of the coarse – graining degree (N_m) on density profiles of the fluid confined by flat surfaces. The degree of coarse-graining is analyzed in the z – direction of the simulation cell, namely perpendicularly to the walls. The main panel in the figure shows the structure induced on the fluid by the wall when varying the magnitude of the parameter N_m on the left side of the simulation cell. These profiles correspond to N_m=1 (black line), N_m=2 (red line), N_m=3 (green line), and N_m=4 (blue line). The full density profiles are presented in the inset. The axes are shown in reduced DPD units.

The influence of the coarse – graining degree on the structure induced in the tangential pressure of the confined fluid is shown in Fig. A2. The amplitude of the layers with respect to the bulk value decreases with N_m, in agreement with the trends seen in Fig. A1, although the extent of these perturbations into the fluid is almost the same in all cases (except for N_m=1), i.e., about five layers before reaching the bulk value.
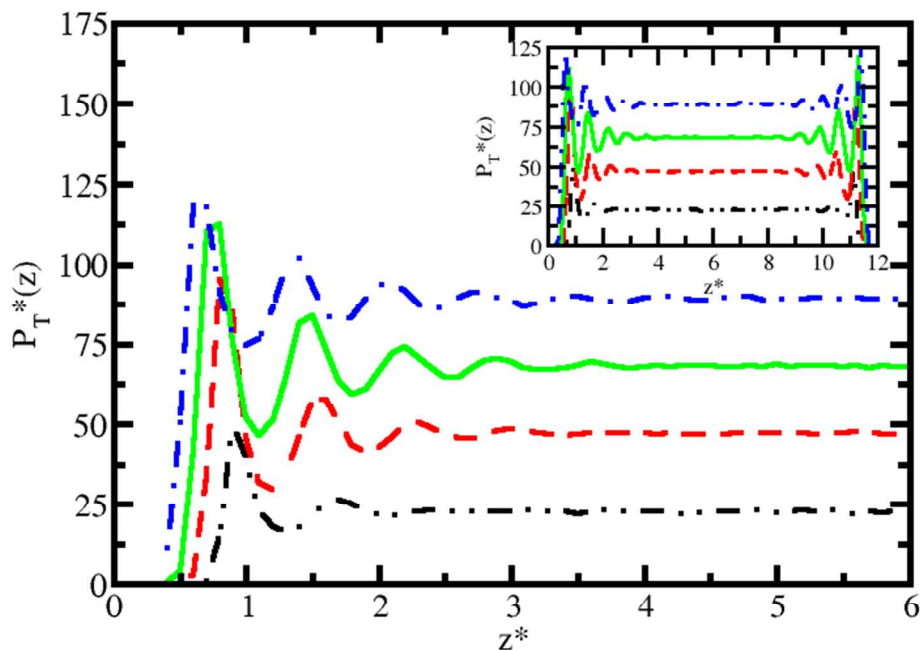
Figure A2. (Color online) Effect of coarse-graining on tangential pressure profiles of the fluid confined by flat surfaces. The degree of coarse-graining is analyzed in the z – direction of the simulation cell, namely perpendicularly to the walls. The main panel in the figure shows the effect of tangential pressure varying the magnitude of the parameter N_m on the left of the simulation cell. The different profiles correspond to $N_m=1$ (black line), $N_m=2$ (red line), $N_m=3$ (green line), and $N_m=4$ (blue line). The total tangential profiles are presented in the inset. The axes are shown in reduced DPD units.
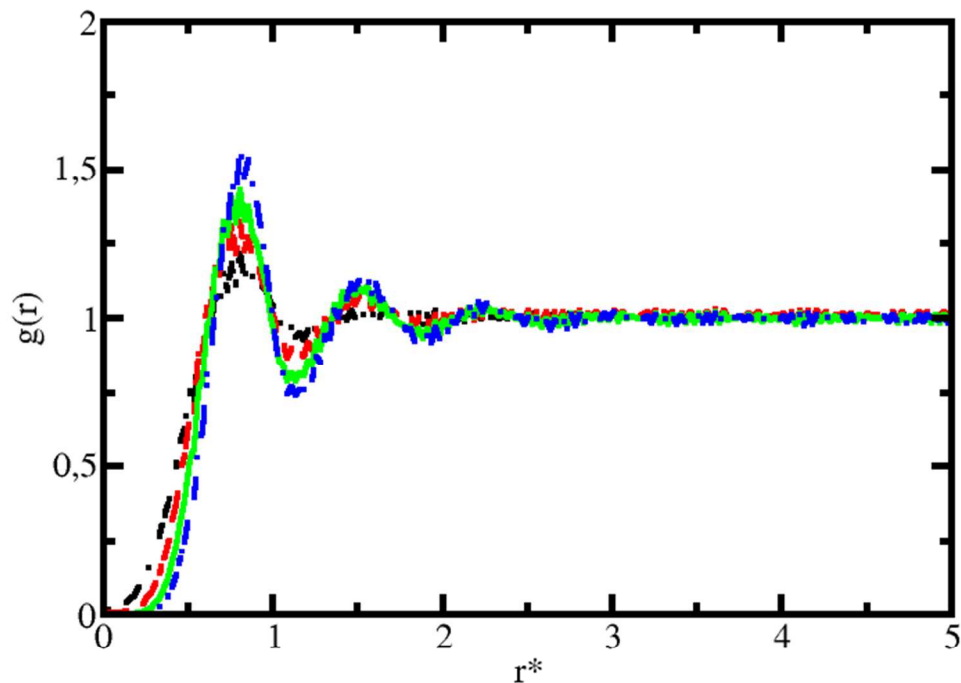
Figure A3. (Color online) Effect of the coarse – graining degree on the two – dimensional (xy – plane) radial distribution function of a confined fluid by flat surfaces. The different profiles correspond to N_m=1 (black line), N_m=2 (red line), N_m=3 (green line), and N_m=4 (blue line). These functions were calculated at a distance $z^* = 1$ from the wall.

In Fig. A3 we show the radial distribution function of the DPD fluid confined by smooth walls in the xy – plane, where the fluid is not confined, for increasing coarse – graining degrees. Although the amplitude of the oscillations is somewhat increased as N_m increases, the extent of structure of the fluid into the bulk is essentially the same in all cases. It should be stressed that the curves shown in Fig. A3 show the *same* structure as that of a fluid which is not confined by walls, as shown in ref. [66].
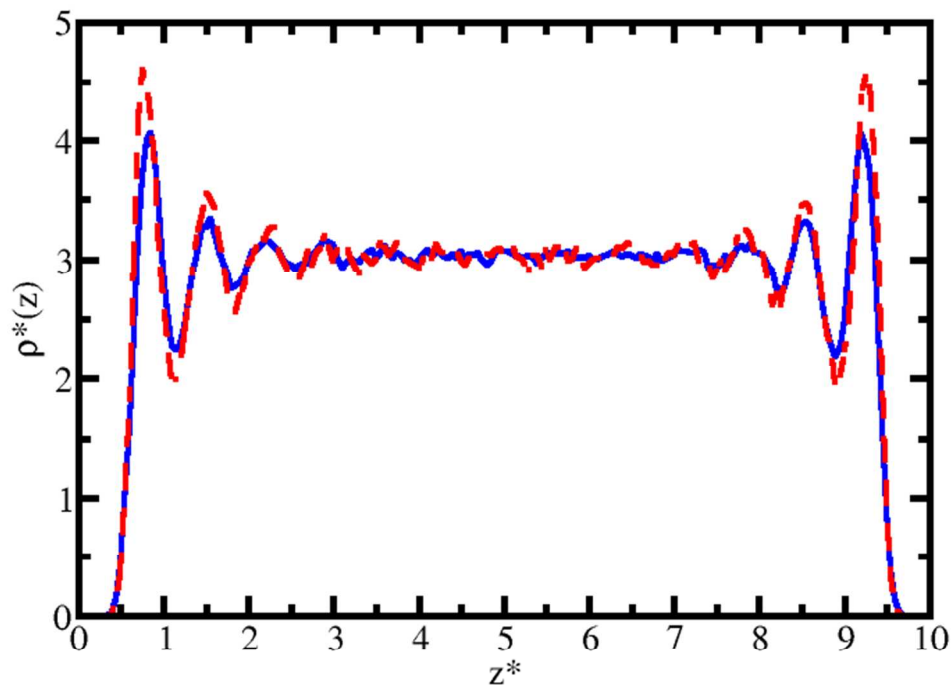
Figure A4. (Color online) Density profiles showing structural changes induced in a fluid confined by surfaces with roughness whose size is smaller than the size of the DPD particles, in the z – direction of the simulation cell, namely perpendicularly to the walls. These profiles were obtained for walls whose roughness parameters are a_R=1.0, $\lambda_1=\pi/4$ (blue line), and $\lambda_1=\pi/8$ (red line), see eq. 3. For both cases shown in this figure we used N_m=3 and the volume of the simulation box was $10\times10\times10$. The axes are shown in reduced DPD units.

Lastly, in Fig. A4 we illustrate how the structuring of the density of the fluid along the direction perpendicular to the walls is modified if the roughness of the walls that confine it is smaller than the size of the fluid's particles. The solid (blue) line in Fig. A4 is taken from the inset in Fig. 3. If the periodicity of the structure on the walls is reduced, the amplitude of the layers in the density profiles grows, until it reaches the limit where the walls are smooth; see for example the green line in Fig. A1. Nevertheless, the period of the oscillations and their extent into the bulk of the fluid are the same for both cases shown in Fig. A4, since those are intrinsic properties of the unbound fluid [68].

References

[1] Becker, T.; Mugele, T. Nanofluidics: Molecularly thin lubricant layers under confinement. *Mol. Sim.* **2005**, 31, 489-494.

[2] Huang, J.; Yan, B.; Faghihnejad, A.; Xu, H.; Zeng, H. Understanding nanorheology and surface forces of confined thin films. *Korea-Australia Rheology Journal*, **2014**, 26, 3-14.

[3] Alba-Simionesco, C.; Coasne, B.; Dosseh, G.; Dudziak, G.; Gubbins, K. E.; Radhakrishnan, R.; Sliwinska-Bartkowiak, M.. Effects of confinement on freezing and melting. *J. Phys.: Condens. Matter* **2006**, 18, R15-R68.

[4] Meyer, E. Atomic force microscopy. *Progress in Surface Science* **1992**, 41, 3-49.

[5] Binnig, G.; Quate, C. F.; Gerber, Ch. Atomic Force Microscope. *Phys. Rev. Lett.* **1986**, 56, 930-933.

[6] Klein, J.; Kumacheva, E.; Mahalu, D.; Perahia, D.; Fetters, L. J. Reduction of frictional forces between solid surfaces bearing polymer brushes. *Nature* **1994**, 370, 634-636

[7] Klein, J.; Kumacheva, E.; Warburg, S. Forces between polymer-bearing surfaces undergoing shear. *Nature* **1991**, 352, 143-145.

[8] Svetovoy, V.B.; Palasantzas, G. Influence of surface roughness on dispersion forces. *Advances in Colloid and Interface Science* **2015**, 216, 1-19.

[9] Cui, S. T.; Cummings, P. T.; Cochran, H. D. Molecular dynamics simulation of the rheological and dynamical properties of a model alkane fluid under confinement. *J. Chem. Phys*. **1999**, 111, 1273-1280.

[10] Cummings, P. T.; Docherty, H.; Iacovella, C. R.; Singh, J. K. Phase transitions in nanoconfined fluids: The evidence from simulation and theory. *AIChE J*. **2010**, 56, 842-848.

[11] Israelachvili, J.; Min, Y.; Akbulut, M.; Alig, A.; Carver, G.; Greene, W.; Kristiansen, K.; Meyer, E.; Pesika, N.; Rosenberg, K.; Zeng, H. *Rep. Prog. Phys*. **2010**, 73, 036601.

[12] Gee, M. L.; McGuiggan, M. P.; Israelachvili, J. N.; Homola, A. M.; Liquid to solidlike transitions of molecularly thin films under shear. *J. Chem. Phys.* **1990**, 93, 1895.

[13] Klein, J.; Kumacheva, E. Simple liquids confined to molecularly thin layers. I. Confinement-induced liquid-to-solid phase transitions. *J. Chem. Phys.* **1998**, 108, 6996.

 [14] Demirel, A. L.; Granick, S. Glasslike. Transition of a Confined Simple Fluid. *Phys. Rev. Lett*. **1996**, 77, 2261.

[15] Granick, S. Motions and Relaxations of Confined Liquids. *Science* **1991**, 253, 1374.

[16] Ohnishi, S.; Kaneko, D.; Gong, J. P.; Osada, Y.; Stewart, A. M.; Yaminsky, V. V. Influence of Cyclohexane Vapor on Stick-Slip Friction between Mica Surfaces. *Langmuir* **2007**, 23, 7032-7038.

[17] Bureau, L. Nonlinear Rheology of a Nanoconfined Simple Fluid. *Phys. Rev. Lett*. **2010**, 104, 218302.

[18] Neto, C., Evans, D. R.; Bonaccurso, E.; Butt. H.; Craig, V. S. J. Boundary slip in Newtonian liquids: a review of experimental studies. *Rep. Prog. Phys*. **2005**, 68, 2859-2897.

[19] Kleinstreuer, C.; Koo J. Computational analysis of wall roughness effects for liquid flow in micro-conduits. *J. Fluids Eng.* **2004**, 126, 1-9.

[20] Sobhan, C. B.; Garimella, S. V. A comparative analysis of studies on heat transfer and fluid flow in microchannels *Microscale Thermophys. Eng.* **2001**, 5, 293-311.

[21] Bock, H.; Schoen M.; Phase behavior of a simple fluid confined between chemically corrugated substrates *Physical Review E*, **1999**, 59, 4122-4136.

[22] Puibasset, J. Phase coexistence in heterogeneous porous media: A new extension to Gibbs ensemble Monte Carlo simulation method. *J. Chem. Phys.,* **2005**, 122, 134710.

[23] Kofke, D. A.; Glandt, E. D. Monte Carlo simulation of multicomponent equilibria in a semigrand canonical ensemble. *Mol. Phys.* **1998**, 64, 1105-1131.

[24] Shi, W.; Zhao, X.; Johnson, J. K. Phase transitions of adsorbed fluids computed from multiple-histogram reweighting. *Mol. Phys.* **2002**, 100, 2139-2150.

[25] De Grandis, V.; Gallo, P.; Rovere, M. Liquid-liquid coexistence in the phase diagram of a fluid confined in fractal porous materials. *Europhys. Lett.* **2006**, 75, 901.

[26] Gruhn, T.; Schoen, M. Grand Canonical ensemble Monte Carlo simulations of confined 'nematic' Gay-Berne films. *Thin Solid Films* **1998**, 330, 46-58.

[27] Dijkstra, M. The effect of branching on the structure of confined thin films of alkanes. *Europhys. Lett.* **1997**, 37, 281-287.

[28] Porcheron, F.; Rousseau, B.; Fuchs, A. H.; Schoen, M. Monte Carlo simulations of nanoconfined n-decane films. *Phys. Chem. Chem. Phys.* **1999**, 1, 4083-4090.

[29] Porcheron, F.; Rousseau, B.; Schoen, M.; Fuchs, A. H. Structure and solvation forces in confined alkane films. *Phys. Chem. Chem. Phys.* **2001**, 3, 1155-1159.

[30] Porcheron, F.; Rousseau, B.; Fuchs, A. H. Structure of ultra-thin confined alkane films from Monte Carlo simulations. *Mol. Phys.* **2002**, 100, 2109-2119.

[31] Porcheron, F.; Schoen, M.; Fuchs, A. H. Monte Carlo simulation of a complex fluid confined to a pore with nanoscopically rough walls. *J. Chem. Phys.* **2002**, 116, 5816-5824.

[32] Puibasset, J. Surface excess free energy of simple fluids confined in cylindrical pores by isothermal-isobaric Monte Carlo: influence of pore size. *J. Chem. Phys.* **2007**, 126, 184701.

[33] Soddemann, T.; Dunweg, B.; Kremer, K. Dissipative particle dynamics: A useful thermostat for equilibrium and nonequilibrium molecular dynamics simulations. *Physical Review E* **2003**, 68, 046702.

[34] Li, Z.; Drazer, G. Hydrodynamic interactions in dissipative particle dynamics. *Phys. Fluids* **2008**, 20, 103601.

[35] Chen, S.; Phan-Thien, N.; Khoo, B. C.; Fan, X. J. Flow around spheres by dissipative particle dynamics. *Physics of Fluids* **2006**, 18, 103605.

[36] Boek, E. S.; Coveney, P. V.; Lekkerkerker, H. N. W.; van der Schoot, P. Simulating the rheology of dense colloidal suspensions using dissipative particle dynamics. *Phys. Rev. E* **1997**, 55, 3124-3133.

[37] Fan X. J.; Phan-Thien, N.; Yong, N. T.; Wu, X.; Xu, D. Microchannel flow of a macromolecular suspension. *Phys. Fluids* **2003**, 15, 11-21.

[38] Goujon, F.; Malfreyt, P.; Tildesley, D. J. Mesoscopic simulation of entangled polymer brushes under shear: compression and rheological properties. *Macromolecules* **2009**, 42, 4310-4318.

[39] Arai, N.; Yasuoka, K.; Zeng, X. C. Nanochanel with uniform and Janus surfaces: shear thinning and thickening in surface solution. *Langmuir* **2012**, 28, 2866-2872.

[40] Kong, Y.; Manke, C. W.; Madden, W. G.; Schlijper, A. G. Simulation of a confined polymer in solution using the dissipative particle dynamics method. *International J. Thermo.* **1994**, 15, 1093-1101.

[41] Liu, H.; Li, Y.; Krause, W. E.; Pasquinelli, M. A.; Rojas, O. J. Mesoscopic simulations of the phase behavior of aqueous $EO_{19}PO_{29}EO_{19}$ solutions confined and sheared by hydrophobic and hydrophilic surfaces. *Appl. Mater. Interfaces* **2012**, 4, 87 − 95.

[42] Liu, K.; Jiang, L. Bio-Inspired Self-Cleaning Surfaces. *Annu. Rev. Mater. Res*. **2012**, 42, 231–63.

[43] Ruths, M.; Israelachvili, J. N. Surface Forces and Nanorheology of Molecularly Thin Films. *Nanotribology and Nanomechanics*, Springer-Verlag Berlin Heidelberg 2011, 107-202.

[44] Español, P.; Warren, P. Statistical Mechanics of Dissipative Particle Dynamics. *Europhys. Lett.* **1995**, 30, 191-196.

[45] Groot, R. D.; Warren, P. B. Dissipative particle dynamics: Bridging the gap between atomistic and mesoscopic simulation. *J. Chem. Phys.* **1997**, 107, 4423-4435.

[46] Maiti, A.; McGrother, S. Bead–bead interaction parameters in dissipative particle dynamics: Relation to bead-size, solubility parameter, and surface tension. *J. Chem. Phys.* **2004**, 120, 1594-1601.

[47] Groot, R. D.; Rabone, K. L. Mesoscopic simulation of cell membrane damage, morphology change and rupture by nonionic surfactants. *Biophys J.* **2001**, 81, 725–736.

[48] Hoogerbrugge, P. J.; Koelman, J. M. V. A. Simulating microscopic hydrodynamic phenomena with dissipative particle dynamics. *Europhys. Lett.* **1992**, 19, 155-160.

[49] Allen, M. P.; Tildesley, D. J. *Computer simulation of liquids* (Clarendon, Oxford, 1987).

[50] Forrest, B. M.; Suter, U. W. Accelerated equilibration of polymer melts by time-coarse-graining. *J. Chem. Phys*. **1995,** 102, 7256-7266.

[51] Frenkel, D.; Smit, B. *Understanding molecular simulation* (Academic, New York, 2002).

[52] Humphrey, W.; Dalke, A.; Schulten, K. VMD - Visual Molecular Dynamics. *J. Molec. Graphics* **1996**, 14, 33-38.

[53] Goicochea, A. G. Adsorption and disjoining pressure isotherms of confined polymers using dissipative particle dynamics. *Langmuir* **2007**, 23, 11656-11663.

[54] Alarcón, F.; Pérez, E.; Goicochea, A G. Dissipative particle dynamics simulations of weak polyelectrolyte adsorption on charged and neutral surfaces as a function of the degree of ionization. *Soft Matter* **2013**, 9, 3777-3788.

[55] Goicochea, A. G.; Nahmad, E.; Pérez, E. Colloidal stability dependence on polymer adsorption through disjoining pressure isotherms. *Langmuir* **2009**, 25, 3529-3537.

[56] Goujon, F.; Malfreyt, P.; Tildesley, D. J. Dissipative particle dynamics simulations in the grand canonical ensemble: applications to polymer brushes. *ChemPhysChem*. **2004**, 5, 457-464.

[57] Gogelein, Ch.; Brinkmann, M.; Schröter, M.; Herminghaus, S. Controlling the Formation of Capillary Bridges in Binary Liquid Mixtures. *Langmuir* **2010**, 26, 17184-17189.

[58] Schmidt, M.; Fortini, A.; Dijkstra, M. Capillary condensation of colloid–polymer mixtures confined between parallel plates. *J. Phys.: Condens. Matter* **2003**, 15, S3411-S3420.

[59] Irving, J. H.; Kirkwood, J. G. The Statistical Mechanical Theory of Transport Processes. IV. The Equations of Hydrodynamics. *J. Chem. Phys.* **1950**, 18, 817-829.

[60] Duda, Y.; Vakarin, E.; Alejandre, J. Stability and interfacial properties of confined nonadditive hard-sphere binary mixture. *Journal of Colloid and Interface Science* **2003**, 258, 10-19.

[61] http://www.simes.uaemex-labs.org.mx/

[62] Vattulainen, I.; Karttunen, M.; Besold, G.; Polson, J. M. Integration schemes for dissipative particle dynamics simulations: From softly interacting systems towards hybrid models. *J. Chem. Phys.*, **2002**, 116, 3967-3979.

[63] Israelachvili, J. N. *Intermolecular and Surfaces Forces* (Academic Press, New York, 2nd edn, 1992).

[64] Schoen, M.; Diestler, D. J.; Cushman, J. H. Stratification – induced order – disorder phase transitions in molecularly thin confined films. *J. Chem. Phys.* **1994**, 101, 6865 – 6873.

[65] Evans, R.; Henderson, J. R.; Hoyle, D. C.; Parry, A. O. and Sabeur, Z. A., Asymptotic decay of liquid structure: oscillatory liquid – vapor density profiles and the Fisher – Widom line. *Mol. Phys.*, **1993**, 80, 755.

[66] Goicochea, A. G.; Alarcón, F. Solvation force induced by short range, exact dissipative particle dynamics effective surfaces on a simple fluid and on polymer brushes. *J. Chem. Phys.*, **2011**, 134, 014703.

[67] Radhakrishnan, R.; Gubbins, K. E. Effect of the fluid-wall interaction on freezing of confined fluids: Toward the development of a global phase diagram. *J. Chem. Phys.*, **2000**, 112, 11048-11057.

[68] Fisher, M. E.; Wiodm, B.; Decay of Correlations in Linear Systems. *J. Chem. Phys.*, **1969**, 50, 3756-3772.

[69] Frink, L. J. D.; van Swol, F. Solvation forces between rough surfaces. *J. Chem. Phys.*, **1998**, 108, 5588-5598.

[70] Ghatak, Ch.; Ayappa, K. G. Solvation force, structure and thermodynamics of fluids confined in geometrically rough pores. *J. Chem. Phys.*, **2004**, 120, 9703-9714.

GRAPHICAL ABSTRACT
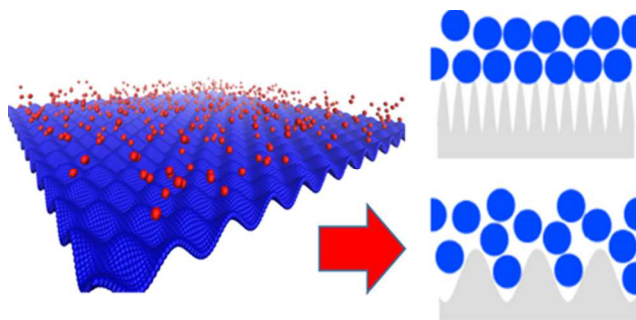
Simulations show that the ordering of particles confined by rough surfaces induces a structural phase transition while the interfacial tension is insensitive to it.

1